Transmitted-acoustic-phonon drag between two-dimensional electron gases in $GaAs/Al_xGa_{1-x}As$ systems at low temperatures: Monte Carlo study

Martin Moško,* Jean-Luc Pelouard, and Fabrice Pardo

Laboratoire de Microstructures et de Microélectronique, CNRS-L2M 196 Avenue Henri Ravéra, Boîte Postale 107, 92225 Bagneux CEDEX, France

(Received 6 July 1994; revised manuscript received 27 March 1995)

We present Monte Carlo simulation of the transmitted-acoustic-phonon (TAP) drag between barrier-separated two-dimensional (2D) electron gases in the $Al_xGa_{1-x}As/GaAs$ systems. Nonequilibrium acoustic phonons emitted by hot 2D electron gas in the biased GaAs channel travel across the sample. These phonons are partially absorbed in an unbiased 2D channel where they induce a drag current. Simulation includes 2D electron–nonequilibrium acoustic-phonon interaction for both deformation-potential and piezoelectric coupling. Nonequilibrium phonon distribution is calculated numerically. The TAP drag is simulated at 4.2 and 2.2 K in a multiple quantum well containing equivalent high-mobility 2D electron gases. Drift velocities around 1000 m/s are found in the drag channel (2D gas without outer field) when it is driven by the TAP drag from a large number (10–50) of 2D electron gases subjected to electric field of 1000 V/m. The TAP drag is mainly due to the deformation-potential coupling. The rate of momentum transfer between the drag channel and drive channels is $\tau_d^{-1} \approx 1.5 \times 10^6$ s^{-1}. We also demonstrate the enhancement of the TAP drag in thin samples due to multiple-phonon reflections from sample surfaces.

I. INTRODUCTION

Two spatially separated gases of free carriers in semiconductors can interact in various ways and with various coupling strengths, depending on their dimensionality, charge, mutual distance, semiconductor material used, etc. Mutual interaction between the gases can lead to the drag effect: *A current flowing in the biased channel (drive current) induces a current (or voltage in case of opened circuit) in the adjacent parallel channel without any external bias voltage.* Hubner and Shockley[1] measured mutual drag between two parallel three-dimensional (3D) electron gases in a silicon crystal. This so-called transmitted acoustic phonon (TAP) drag was due to the emission of nonequilibrium acoustic phonons by the biased electron gas and absorption of these phonons by the other electron gas. Coulomb drag between carrier gases of various dimensionalities has been investigated in $GaAs/Al_xGa_{1-x}As$ systems.[2–15] The drag between two 2D electron gases in the double quantum well (DQW) was measured[10–12] for various distances between the gases at temperatures 1–7 K. For small distances (17.5 and 22.5 nm) Coulomb interaction was the dominant drag mechanism.[10,11] For large distances (50 and 500 nm) the drag was due to the virtual-acoustic phonon exchange between the gases,[12,13] while the TAP drag was concluded to be negligible. Nevertheless, there is an indirect indication that the TAP drag is observable also in $Al_xGa_{1-x}/GaAs$ systems. Karl *et al.*[16] observed the drag of the 2D electron gas, due to acoustic phonons emitted from a laser-irradiated Al layer. It seems natural to think over a similar experiment, where the source of phonons would be the 2D electron gas driven by electric field. Qualitative considerations have been presented by Price,[17] but a detailed calculation would be useful to specify proper experimental conditions and to stimulate further experimental work. We report on such calculations in our paper. We present Monte Carlo (MC) simulation of the TAP drag between parallel 2D electron gases in $GaAs/Al_xGa_{1-x}As$ systems at 4.2 and 2.2 K. In perfectly Ohmic conditions,[10–12] for electric field in the drive channel (F) less than 1 V/m, the TAP drag is negligible. We consider $F = 1000$ V/m and deal with hot electron transport accompanied by strong emission of hot acoustic phonons from the drive channel. Instead of the DQW,[10–12] we consider the multiple quantum well (MQW), in which one 2D electron gas is driven by the TAP drag from a large number of the drive channels. The TAP drag is proportional to the number of the drive channels, which is not the case for the Coulomb and virtual-phonon drag. Unlike to Ohmic conditions,[12] the TAP drag in the hot electron regime is mainly due to the deformation-potential coupling and its dependence on temperature is negligible in the Bloch-Grüneisen regime. We also demonstrate the enhancement of the TAP drag in thin samples, due to multiple phonon reflections from sample surfaces.

In Sec. II, the simulation of 2D electron-acoustic-phonon scattering is developed for both deformation-potential and piezoelectric interactions. Electron interactions with polar-optic phonons, with imperfections of the host crystal and with other electrons are considered as well. In Sec. III, we calculate nonequilibrium acoustic-phonon distribution and the TAP drag in the MQW structure with infinitely thick substrate, in Sec. IV, we analyze thin samples. In Sec. V, we discuss limitations of our model. A summary is given in Sec. VI.

II. TRANSPORT MODEL AND MC ALGORITHM

In Fig. 1, we show the periodic MQW considered in our analysis. The widths of the wells (L_W) and barriers (L_B) are 20 and 200 nm, respectively. The sample boundaries are located at $z = 0$ and $z = L_S$. Each well is occupied by the electron gas of sheet density $n_s = 1.5 \times 10^{11}$ cm^{-2}. Assuming that the GaAs layer z_1 is contacted separately from the GaAs layers $z_2, ..., z_{N_W}$, we consider parallel electric field F only in quantum wells $z_2, ..., z_{N_W}$, which serve as drive channels. Quantum well z_1 is without electric field and serves as a drag channel. Electrons are assumed to occupy only the lowest energy subband, described by sine envelope function in the flat band approximation.[18] Occupation of higher subbands and real-space electron transfer in the drive channels can be neglected (see Sec. V). In the individual quantum well, the 2D motion of N electrons (typically $N = 10\,000 - 60\,000$) is simulated using ensemble MC simulation.[19] Besides electron interaction with bulk polar-optic phonons,[19] we include the following scattering mechanisms.

The e-e scattering is modeled like two-particle Coulomb collisions described by the Fermi golden rule.[19–21] The interwell e-e scattering which can cause Coulomb drag between the wells z_1 and z_2 (Refs. 21 and 22) can be neglected for $L_B = 200$ nm, while the intrawell e-e scattering slightly affects the hot electron drift velocity.[21,22] Scattering due to the imperfections of the host crystal (residual impurities, interface roughness, remote donors) cannot be neglected at low temperatures. We simulate these mechanisms as isotropic and elastic scattering of the frequency $\tau_I^{-1} = e/(m\mu_I)$,[23] where m is the electron effective mass and μ_I is the electron mobility limited only by the imperfections. At $T < 1$ K, because the phonon scattering is negligible, μ_I is the same as the measured $\mu = 3.5 \times 10^6$ cm^2 V^{-1} s^{-1}.[10–12] At higher T, μ_I remains temperature independent as far as the 2D gas is strongly degenerate[23] (the case of the drag channel) and $\tau_I^{-1} = e/(m\mu_I) = 7.5 \times 10^9$ s^{-1}. In "hot electron" drive channels, this simplified approach becomes rough; the error is, however, not serious because hot electron momenta are relaxed mainly by phonon scattering.

To take into account degeneracy, the electron state after the collision, $\mathbf{k}_0$, is accepted if the electron occupation number $f(\mathbf{k}_0)$ is less than a number randomly chosen between 0 and 1, otherwise self-scattering occurs. If the 2D gas is strongly degenerate, it is not sufficient to calculate $f(\mathbf{k}_0)$ in discrete points of the $\mathbf{k}$ space,[20–24] because $f(\mathbf{k}_0)$ varies too rapidly in the vicinity of the Fermi energy states [test simulations of equilibrium dynamics show unphysical deviations of $f(\mathbf{k}_0)$ from the initial equilibrium Fermi distribution with progressing time, when 4.2 K$< T <$ 30 K]. Therefore, we use discrete numerical tabulation[24] of $f(\mathbf{k}_0)$ only for a hot electron gas with electron temperature $T_e > 30$ K. For $T_e < 30$ K ,we take $f(\mathbf{k}_0)$ as a heated shifted Fermi distribution, because such an analytical distribution prevents the mentioned unphysical effect when $T_e \to T$. $f(\mathbf{k}_0)$ is updated after each 500 fs and the same time step is used for the finite time discretization.

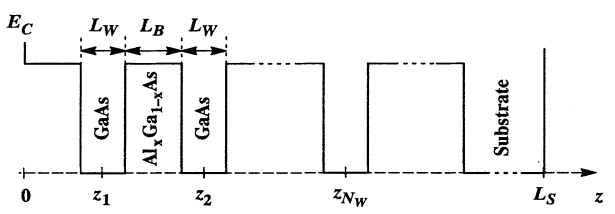

FIG. 1. Conduction band edge E_c and geometry of the simulated MQW.

The 2D electron-acoustic-phonon scattering rate of an electron in state $\mathbf{k}$ is[25]

$$\lambda^{\pm}(\mathbf{k}) = \frac{1}{8\pi^2\rho}\int d\mathbf{Q}\int dq_z \frac{C^2(\mathbf{q})}{v_s q \varepsilon^2(Q)}\left[n(\mathbf{q}) + \frac{1}{2} \pm \frac{1}{2}\right] \times \delta_{\mathbf{k},\mathbf{k}_0 \pm \mathbf{Q}}\,\delta\left(\frac{\hbar^2 k^2}{2m} - \frac{\hbar^2 k_0^2}{2m} \pm \hbar v_s q\right) \mid S_0(q_z) \mid^2, \tag{1}$$

where ρ is the density of the crystal, v_s is the velocity of sound, $\mathbf{q} = (\mathbf{Q}, q_z)$ is the phonon-wave vector, $\mathbf{Q}$ is the in-plane component of $\mathbf{q}$, $C^2(\mathbf{q})$ is the coupling strength, $n(\mathbf{q})$ is the phonon distribution function, $\varepsilon(Q)$ is the screening function, and

$$S_0(q_z) = (2/L_W)\int_0^{L_W} dz\; e^{iq_z z}\; \sin^2(\pi z/L_W). \tag{2}$$

The upper (lower) signs in (1) hold for the emission rate λ^+ (absorption rate λ^-). Interactions with longitudinal phonons are[26] due to deformation potential, with

$$C^2(\mathbf{q}) = D^2 q^2, \tag{3}$$

and piezoelectric coupling, with

$$C^2(\mathbf{q}) = 4(eh_{14}/\varepsilon_s)^2(3\alpha\beta\gamma)^2. \tag{4}$$

Here, D is the deformation-potential constant, h_{14} is the piezoelectric tensor component, ε_s is the static permitivity, and α, β, and γ are the directions cosines of the vector $\mathbf{q}$ with respect to the crystal axes. Electron interactions with both transverse phonon modes are[26] due to the piezoelectric coupling, with

$$C^2(\mathbf{q}) = 4(eh_{14}/\varepsilon_s)^2\left[\alpha^2\beta^2 + \beta^2\gamma^2 + \gamma^2\alpha^2 - (3\alpha\beta\gamma)^2\right]. \tag{5}$$

Assuming the orientation of the GaAs layers in the [0 0 1] direction and the field $\mathbf{F} = (F, 0, 0)$ parallel to the direction [1 0 0], we use $\alpha = q_x/q$, $\beta = q_y/q$, and $\gamma = q_z/q$. Screening function $\varepsilon(Q)$ is taken in static screening approximation as

$$\varepsilon(Q) = 1 + H(Q)\frac{Q_n}{Q}, \tag{6}$$

where $H(Q)$ is the form factor [see, e.g., Ref. 19, formula (2.1)] and Q_n is the electron temperature dependent 2D screening constant,[21] updated after each 500 fs.

Integrating over q_z and introducing polar coordinates Q and ϕ (with ϕ being the angle between $\mathbf{k}$ and $\mathbf{Q}$), we obtain from (1) for $k > mv_s/\hbar$ the expressions

$$\lambda^+(\mathbf{k}) = \frac{1}{8\pi^2\hbar\rho v_s^2} \int_{Q^+_{\min}}^{Q^+_{\max}} dQ \int_{-\phi^+}^{\phi^+} d\phi\, P^+(Q,\phi,k), \tag{7}$$

$$\lambda^-(\mathbf{k}) = \frac{1}{8\pi^2\hbar\rho v_s^2} \left\{ \int_{Q^-_{\min}}^{Q^-_{\max}} dQ \int_{-\phi^-}^{\phi^-} d\phi\, P^-(Q,\phi,k) + \int_{Q^-_{\max}}^{\infty} dQ \int_{-\pi}^{\pi} d\phi\, P^-(Q,\phi,k) \right\}, \tag{8}$$

where

$$Q^\pm_{\min} = 0\,, \quad Q^\pm_{\max} = 2k\left(1 \pm \frac{mv_s}{\hbar k}\right)\,, \qquad \phi^\pm = \arccos\left(\frac{Q}{2k} \pm \frac{mv_s}{\hbar k}\right), \tag{9}$$

$$P^\pm(Q,\phi,k) = \frac{Q}{q_z^\pm}\, C^2(Q,\phi,q_z^\pm)\, \frac{|\,S_0(q_z^\pm)\,|^2}{\varepsilon^2(Q)} \left[n(q,\phi,q_z^\pm) + n(Q,\phi,-q_z^\pm) + 1 \pm 1\right], \tag{10}$$

$$q_z^\pm = \sqrt{\left(\frac{\hbar kQ}{mv_s}\cos\phi \mp \frac{\hbar Q^2}{2mv_s}\right)^2 - Q^2}\,. \tag{11}$$

For $k < mv_s/\hbar$, we find $\lambda^+(\mathbf{k}) = 0$, but $\lambda^-(\mathbf{k})$ is given by (8), except that $Q^-_{\min} = 2k(\frac{mv_s}{\hbar k} - 1)$. Integration limits in (7) and (8) were obtained from the inequality $2k\cos\phi \mp Q^2 \geq 0$, which ensures the decrease (for emission) or the increase (for absorption) of the electron energy in the scattering event, and from $(\frac{\hbar kQ}{mv_s}\cos\phi \mp \frac{\hbar Q^2}{2mv_s})^2 \geq Q^2$.

Scattering rates $\lambda^\pm(\mathbf{k})$ can be used together with other scattering rates in the MC selection[19] of the electron-free flight time and scattering channel. When the acoustic-phonon scattering is selected, one needs to select the in-plane wave vector $\mathbf{Q}$ of the phonon involved in the scattering event and to compute final electron state, $\mathbf{k}_0 = \mathbf{k} \mp \mathbf{Q}$, after the scattering. In the MC method, vector $\mathbf{Q}$ can be viewed as a pair of random variables Q, ϕ, distributed in the integration limits of integrals (7) and (8) according to the (unnormalized) probability distribution $P^\pm(Q,\phi,k)$.

In case of phonon emission, Q and ϕ can be generated by solving the equations

$$r_1\lambda^+(\mathbf{k}) = \frac{1}{8\pi^2\hbar\rho v_s^2} \int_{Q^+_{\min}}^{Q} dQ' \int_{-\phi^+(Q')}^{\phi^+(Q')} d\phi\, P^+(Q',\phi,k)\,, \tag{12}$$

$$r_2 \int_{-\phi^+(Q)}^{\phi^+(Q)} d\phi'\, P^+(Q,\phi',k) = \int_{-\phi^+(Q)}^{\phi} d\phi'\, P^+(Q,\phi',k)\,, \tag{13}$$

where r_1, r_2 are random numbers between 0 and 1. One has first to calculate $Q = Q(r_1)$ from (12) and then $\phi = \phi(r_2, Q)$ from (13).

In case of phonon absorption one can generate $Q = Q(r_1)$ from the equations

$$r_1\lambda^-(\mathbf{k}) = \frac{1}{8\pi^2\hbar\rho v_s^2} \int_{Q^-_{\min}}^{Q} dQ' \int_{-\phi^-(Q')}^{\phi^-(Q')} d\phi\, P^-(Q',\phi,k)\,, \quad Q \leq Q^-_{\max}\,, \tag{14}$$

$$r_1\lambda^-(\mathbf{k}) = \frac{1}{8\pi^2\hbar\rho v_s^2} \left\{ \int_{Q^-_{\min}}^{Q^-_{\max}} dQ' \int_{-\phi^-(Q')}^{\phi^-(Q')} d\phi\, P^-(Q',\phi,k) + \int_{Q^-_{\max}}^{Q} dQ' \int_{-\pi}^{\pi} d\phi\, P^-(Q',\phi,k) \right\}, \quad Q > Q^-_{\max}\,, \tag{15}$$

and then $\phi = \phi(r_2, Q)$ from the equations

$$r_2 \int_{-\phi^-(Q)}^{\phi^-(Q)} d\phi'\, P^-(Q,\phi',k) = \int_{-\phi^-(Q)}^{\phi} d\phi'\, P^-(Q,\phi',k), \quad Q \leq Q^-_{\max}\,, \tag{16}$$

$$r_2 \int_{-\pi}^{\pi} d\phi'\, P^-(Q,\phi',k) = \int_{-\pi}^{\phi} d\phi'\, P^-(Q,\phi',k)\,, \quad Q > Q^-_{\max}\,. \tag{17}$$

Direct numerical solution of (12)–(17) would be too difficult especially when $P^{\pm}(Q,\phi,k)$ varies during the simulation [$n(\mathbf{q})$ in $P^{\pm}(Q,\phi,k)$ is not known *a priori* and has to be determined in the simulation]. To avoid these problems, we developed a special "self-scattering" technique. Let us assume that $P^{\pm}(Q,\phi,k)$ is replaced in (7), (8), (12)–(17) by an artificially constructed analytical distribution $B^{\pm}(Q,\phi,k)$, which obeys the inequality $B^{\pm}(Q,\phi,k) > P^{\pm}(Q,\phi,k)$ and yields analytical expression for $Q(r_1)$, $\phi(r_2)$, and $\lambda^{\pm}(k)$. Assume now that simulation of acoustic-phonon scattering is performed with these analytical expressions. This simple simulation is incorrect, because the free flight of an electron in state $\mathbf{k}$ is interrupted with the collisional frequency, overestimated for given Q and ϕ by a factor of $B^{\pm}(Q,\phi,k)/P^{\pm}(Q,\phi,k)$. A correct simulation can be achieved as follows. After the electron-free flight was interrupted by acoustic-phonon scattering and the values of $Q(r_1)$ and $\phi(r_2)$ were generated, it is necessary to test the inequality,

$$r < \frac{P^{\pm}\Big(Q(r_1),\phi(r_2),k\Big)}{B^{\pm}\Big(Q(r_1),\phi(r_2),k\Big)} , \tag{18}$$

where r is a random number selected between 0 and 1. If (18) is fulfilled, generated values of Q and ϕ are accepted and electron is scattered ($\mathbf{k}_0 = \mathbf{k} \pm \mathbf{Q}$), otherwise self-scattering occurs ($\mathbf{k}_0 = \mathbf{k}$) and electron remains unscattered. Since (18) can be fulfilled with probability $P^{\pm}/B^{\pm}$, the self-scattering reduces the frequency of real collisions with given Q and ϕ by a factor of $P^{\pm}(Q,\phi,k)/B^{\pm}(Q,\phi,k)$. This reduction exactly cancels the above discussed overestimation due to the replacement of $P^{\pm}$ by $B^{\pm}$, i.e., the proposed procedure simulates phonon scattering described by distribution $P^{\pm}(Q,\phi,k)$. The choice of $B^{\pm}$ determines just the frequency of self-scattering events, which has no effect on final results. However, it is not easy to choose a proper $B^{\pm}(Q,\phi,k)$. A constant $B^{\pm}$ would not be the correct choice, because $P^{\pm}(Q,\phi,k)$ diverges for $\phi \to \phi^{\pm}(Q)$ and inequality $B^{\pm}(Q,\phi,k) > P^{\pm}(Q,\phi,k)$ cannot be fulfilled. Furthermore, it is not possible to derive analytical expressions for $Q(r_1)$ and $\lambda^{\pm}(k)$ even in the simplest case [when $B^{\pm}(Q,\phi,k)$ is constant]. In Appendixes A and B, we derive the function $B^{\pm}(Q,\phi,k)$, which provides $\phi(r_2)$ analytically and allows a manageable numerical calculation of $Q(r_1)$ and $\lambda^{\pm}(k)$.

Our technique incorporates inelastic collisions, as well as the anisotropy of piezoelectric coupling without customary approximations,[25,27] and nonequilibrium phonon effects (Secs. III, IV) can also be included. We use generally adopted parameters of the GaAs material[25,27] (the transverse sound velocity is taken from Ref. 28). The deformation-potential D is typically in the range 7–13.5 eV.[23,25] To establish a proper D, we applied our MC technique to the calculation of Ohmic mobility μ at 4.2 K. Using $D = 13.5$ eV, we found the acoustic-phonon-limited mobility $\mu \simeq 8 \times 10^6$ cm^{-2}/V s and total mobility $\mu \simeq 2.5 \times 10^6$ cm^{-2}/V s (Fig. 2 in Ref. 29). The latter value agrees with the measured $\mu(4.2\ \text{K}) = 2.4 \times 10^6$ cm^{-2}/V s.[10,11] As discussed before, the scattering rate, due to imperfections of the host crystal, τ_I^{-1}, is chosen to fit the measured $\mu = 3.5 \times 10^6$ cm^{-2}/V s at $T < 1$ K.[10,11]

III. NONEQUILIBRIUM PHONONS AND THE TAP DRAG IN THE MQW STRUCTURE

We put $n(\mathbf{q}) = n_0(q) + g(\mathbf{q})$, where $n_0(q)$ is the Bose distribution and $g(\mathbf{q})$ is the nonequilibrium part of $n(\mathbf{q})$. To calculate $g(\mathbf{q})$ numerically, we divide $\mathbf{q}$ space into a three-dimensional grid with mesh cells Δq^3, where $\Delta q = 2.5 \times 10^5$ cm^{-1}. During time steps Δt, we count (for each phonon branch separately) the histogram $N_h(\mathbf{q})$—the difference between the numbers of emitted and absorbed phonons in each mesh cell, where $\mathbf{q}$ is the cell center position. The phonon-2D electron collisional integral can be expressed as

$$G(\mathbf{q}) = \left(\frac{2\pi}{\Delta q}\right)^3 \left(\frac{n_s}{N}\right) \frac{N_h(\mathbf{q})}{\Delta t} . \tag{19}$$

Derivation of g requires some simplifying assumptions. At low temperatures in the MQW structures similar to that in Fig. 1 the phonon mean free path, due to bulk nonelectronic scatterers (other phonons, impurities, layer interfaces), l_{ph}, is about 1 mm.[30] When the substrate thickness $\gg l_{\text{ph}}$ (*which we assume*), those excess phonons which succeeded in escaping into the substrate, can no longer return into the region $z \le z_{N_W}$, because they are thermalized by nonelectronic scatterers in the substrate. Therefore excess phonons can cross the region $z \le z_{N_W}$ at most two times when a *specular phonon reflection from the surface* $z = 0$ (Ref. 30) *is assumed.* Since $z_{N_W} \approx 1 - 10$ μm$\ll l_{\text{ph}}$, *excess phonons can be assumed to cross the region* $z \le z_{N_W}$, *without being scattered by nonelectronic scatterers.* Further, two assumptions are *that* $G(\mathbf{q})$ *is the same in each drive channel and negligible in the drag channel.* The latter assumption is based on the fact that cold electrons in the drag channel are scattered by phonons much less frequently than hot electrons in the drive channels. The former assumption is based on the expectation that hot electrons in the drive channels contribute to $G(\mathbf{q})$ mainly through the spontaneous (channel-position independent) phonon emission. Checking this expectation in the simulation, we found that the phonon absorption (including the g-dependent absorption of excess phonons) in an individual drive channel is one order of magnitude less frequent than phonon emission for N_W as large as 51 (i.e., an excess phonon could only be reabsorbed with probability ~ 0.1, when crossing 50 drive channels). Finally, due to symmetry of the spontaneous-emission process in square quantum well, *we assume that* $G(q_x,q_y,q_z) = G(q_x,q_y,-q_z)$. We express $g(\mathbf{q})$ in conditions of steady-state transport.

In the drag channel, the z component of the current density of excess phonons with wave vectors $\mathbf{q}$ in volume Δq^3 can be expressed as $(N_W - 1)(v_z/|v_z|)G(\mathbf{q})(\Delta q/2\pi)^3$, where $v_z = v_s(q_z/q)$. A comparison with the equivalent expression $v_z g(\mathbf{q})(\Delta q/2\pi)^3$ gives

$$g(\mathbf{q}) = (N_W - 1)\frac{G(\mathbf{q})}{\mid v_z \mid} \ . \tag{20}$$

Similarly one can find $g(\mathbf{q})$ in the drive channels. Since for each channel one finds different g, one should simulate, electron transport in each channel. For simplicity, we simulated electron transport in one "representative" drive channel and in the drag channel. In the drag channel, we used (20), while in the "representative" drive channel, we tried (20), $g(\mathbf{q}) \equiv 0$, and also $g(\mathbf{q})$ derived for channel N_W. Numerical results for $G(\mathbf{q})$ were close in all three cases, because the main contribution to the histogram $N_h(\mathbf{q})$ was due to the spontaneous (g-independent) phonon emission. Thus, we only present results obtained using (20) in both simulated channels. Using (20) in the "representative" drive channel, we have $g(q_z) = g(-q_z)$ in all drive channels, which is not the case (for example, channel N_W can only be irradiated by excess phonons with positive q_z). We note that the effect of this inconsistency is small. Each drive channel produces excess phonons with distribution $G(\mathbf{q})/\mid v_z \mid$. The contribution of these phonons to electron scattering in other channels is the same for $q_z > 0$, as well as for $q_z < 0$, because $G(q_x, q_y, q_z) = G(q_x, q_y, -g_z)$. This is not the case only for too large N_W, when G strongly depends on g.

(20) neglects the effect of thermalizing phonon collisions with nonelectronic scatterers in the region $z \leq z_{N_W}$. This approximation cannot be applied to excess phonons with very small v_z, when the transit time $2z_{N_W}/\mid v_z \mid$ becomes larger than the lifetime $l_{\rm ph}/v_s$, and distribution (20), therefore, shows unphysical divergency for $v_z \to 0$. In fact, this problem is not present in a realistic device with the finite distance between the contacts supplying electric field [$d_c \approx 200$ μm (Ref. 10)]. Since $z_{N_W} \ll d_c < l_{\rm ph}$, phonons with very small v_z overcome the distance d_c without being scattered by nonelectronic scatterers. In a rigorous treatment with the effect of finite d_c taken into account, $g(\mathbf{q})$ has to depend on phonon position between the contacts. We adopt a simpler approach by neglecting those "small v_z" phonons for which the position dependence could be important. We expect that the effect of finite d_c is unimportant for $z_{N_W}/\mid v_z \mid \ll d_c/v_s$, but important for $z_{N_W}/\mid v_z \mid > d_c/v_s$. We exclude from the histogram $N_h(\mathbf{q})$ all the phonons with $v_z < v_{z_{\rm min}}$, where $v_{z_{\rm min}}$ is defined by the relation $z_{N_W}/v_{z_{\rm min}} = 0.2d_c/v_z$. Assuming $d_c = 100z_{N_W}$, we have $v_{z_{\rm min}} = v_s/20$. Due to this cutoff, our approach rather underestimates the realistic TAP drag. Another approach (Sec. IV), which ignores finite d_c and takes into account finite lifetime $l_{\rm ph}/v_s$, gives about a 20% stronger TAP drag. The use of a reasonable cutoff $v_{z_{\rm min}}$ is, however, appropriate for $z_{N_W} \ll d_c < l_{\rm ph}$, because the phonons with too small v_z escape the region between the contacts without crossing the drag channel.

In the simulation, we update $g(\mathbf{q})$ after the steps $\Delta t =$ 25 ps, starting with $g = 0$. After 500 ps the transport in the drive channels becomes stationary, and $g(\mathbf{q})$ is then averaged over all following time steps in order to reduce noise. *$g(\mathbf{q})$ converges towards a stable solution within the same time as hot electrons need to reach the steady state. The initial transient effects in the electron-phonon system are artificially accelerated, due to the use of steady-state distribution (20). Realistic phonon transients would be much longer.*

Figure 2 shows the simulated TAP drag for the MQW's with $N_W = 11$, 36, and 51. Here, we neglect electron interactions with the imperfections of the host crystal. An electric field of 1000 V/m is applied to the drive channels $z_2, ..., z_{N_W}$, while the drag channel z_1 is without electric field. Within the fluctuations (the biggest ones for $N_W = 51$, with only 10 000 particles per channel), the saturation value of the "drag" velocity (electron velocity in the drag channel) increases linearly with N_W. This is not the case for Coulomb and virtual-phonon drag, which tend to diminish with increasing distance between the drag and drive channels.[10–12] The momentum transfer rate τ_d^{-1} between a single-drive channel and drag channel z_1 can be estimated from the relation

$$v_2 \ = \ \mu\Big(\frac{mv_1}{e\tau_d}\Big)(N_W - 1) \ . \tag{21}$$

Here, v_2 and v_1 are the "drag" and "drive" velocities in steady state. Taking $\mu = 8 \times 10^6$ cm^2 V^{-1} s^{-1} (see Sec. II), we find $\tau_d^{-1} \simeq 1.5 \times 10^6$ s^{-1} for all three N_W. Figure 3 shows nonequilibrium part $g(q_x)$ and the Bose part $n_0(q_x)$ of the acoustic-phonon distribution $n(q_x) = n_0(q_x) + g(q_x)$ in the drag channel, with $n(q_x)$ normalized to phonon density $\int_{-\infty}^{\infty} dq_x n(q_x)$. The q_z dependence is shown as well. Let us compare transverse and longitudinal distributions. For transverse phonons $g(q_x) \ll n_0(q_x)$. This suggests that piezoelectric interaction with nonequilibrium transverse phonons gives a small contribution to the TAP drag in Fig. 2. We checked that the TAP drag is essentially the same, when only equilibrium transverse phonons are considered. The main contribution to the TAP drag comes from longitudinal phonons for which $g(q_x)$ is comparable

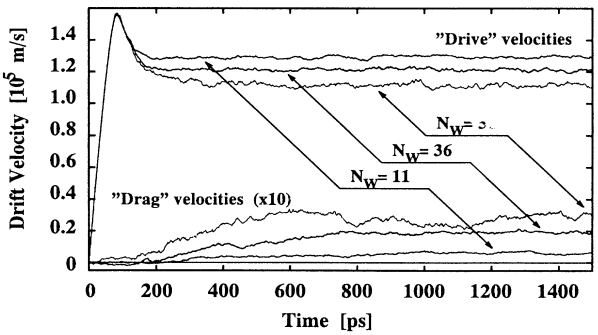

FIG. 2. Drift velocity vs time in the MQW at 4.2 K for $N_W = 11$, 36, and 51. Quantum well z_1 is without electric field, quantum wells $z_2, ..., z_{N_W}$ are with a parallel field $F = 1000$ V/m. "Drive" velocity is the velocity in the wells $z_2, ..., z_{N_W}$. "Drag" velocity (extended by 10) is the velocity in the well z_1. The results were obtained taking $\tau_I^{-1} = 0$. The same number of particles was used in the drive and drag channel: 40 000 for $N_W = 11$, 22 500 for $N_W = 36$, and 10 000 for $N_W = 51$.

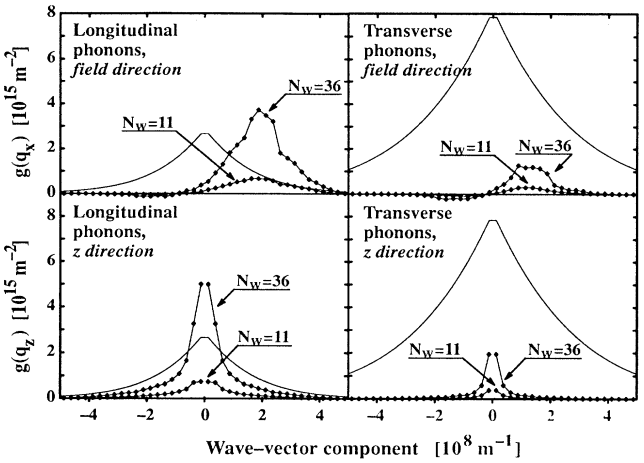

FIG. 3. Acoustic-phonon distribution vs phonon-wave vector in the field direction (q_x) and z direction (q_z). Nonequilibrium part g of the distribution is shown for $N_W = 11$ and 36 (centered symbols connected by full lines). Equilibrium Bose distribution n_0 is shown in a full line. Distributions $g(q_x)$ and $g(q_z)$ were obtained in the same MC run as the results from Fig. 2.

to $n_0(q_x)$. For these phonons, deformation-potential coupling is much more important than piezoelectric coupling: when deformation-potential coupling in each well was restricted to equilibrium phonons, we found $g(q_x) \ll n_0(q_x)$ and the TAP drag was not detectable.

In Fig. 2, one sees the decrease of the "drive" velocity with increasing N_W. A detailed understanding of this friction requires some simulations beyond our computational possibilities, so we only give a brief discussion. The electron friction due to hot phonons with forward drift has already been demonstrated for optical phonons in bulk GaAs (Fig. 13 in Ref. 31) and for acoustic phonons in bulk Ge.[32] The interaction of hot phonons with drifting hot electrons causes the drag effect, but also dissipates the electron momenta. The friction appears when the latter effect prevails.[31,32] Since the friction is due to hot phonons, it tends to diminish with the decreasing hot phonon population, i.e., with the decreasing N_W in the case of Fig. 2. For $N_W = 11$, the "drive" velocity is close to the results (not shown here) obtained for $N_W = 2$ or for $n(\mathbf{q}) \to n_0(\mathbf{q})$. In Ref. 33, it was shown for multiple heterojunction that the phonon drag enhances the low-temperature lattice-scattering limited mobility with increasing N_W. For $N_W \gg 1$, a zero electron-phonon resistance (infinite mobility) appeared,[33] due to the neglect of phonon thermalization by bulk nonelectronic scatterers. Since the phonon thermalization is neglected also in our model, the increase of the friction with N_W in Fig. 2 may seem in contradiction with Ref. 33. In fact, in our model the zero electron-phonon resistance cannot appear, because the decay of excess phonons in the region $z \le z_{N_W}$ is realized through the phonon escape into the thick substrate. This decay mechanism does not exist in thin samples considered in Ref. 33.

In Fig. 5, the TAP drag in the MQW with $N_W = 36$ is calculated including electron interaction with imperfections of the host crystal, i.e., taking $\tau_I^{-1} = 7.5 \times 10^9\ \mathrm{s}^{-1}$. The "drive" velocity is decreased only 22%, because hot electrons relax their momenta mainly through spontaneous phonon emission. The "drag" velocity is, however, reduced about three times. This decrease is consistent with the decrease of electron mobility μ, which is reduced by a factor of 3.2 (from 8×10^6 cm^2/V s to 2.5×10^6 cm^2/V s; see Sec. II). Consequently, estimation of τ_d^{-1} from relation (21) gives nearly the same value ($\sim 1.5 \times 10^6\ \mathrm{s}^{-1}$) like for $\tau_I^{-1} = 0$. In other words, imperfections of the host crystal reduce the "drag" velocity mainly by reducing μ, rather than τ_d^{-1}. To support this interpretation, in Fig. 5, we compare g for $\tau_I^{-1} = 0$ and $7.5 \times 10^9\ \mathrm{s}^{-1}$. In the latter case, g is about 20% smaller and can only cause about 20% decrease of the "drag" velocity.

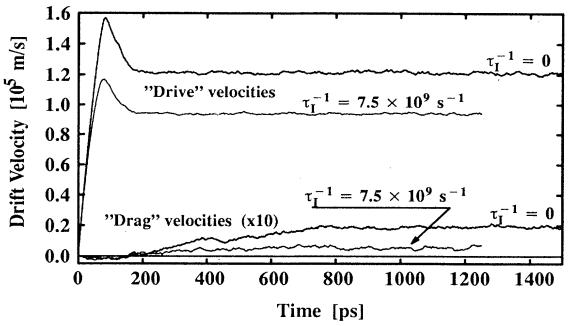

FIG. 4. The same as in Fig. 2 for $N_W = 36$, but the result obtained for $\tau_I^{-1} = 7.5 \times 10^9\ \mathrm{s}^{-1}$ is also shown (60 000 particles per chanel were simulated here).

In Fig. 6, the TAP drag in the MQW with $N_W = 36$ is compared for T =4.2 K and T=2.2 K. We use $\tau_I^{-1} = 7.5 \times 10^9\ \mathrm{s}^{-1}$ to include electron interactions with imperfections of the host crystal. An important result is the very small change of the drift velocities with T. Also

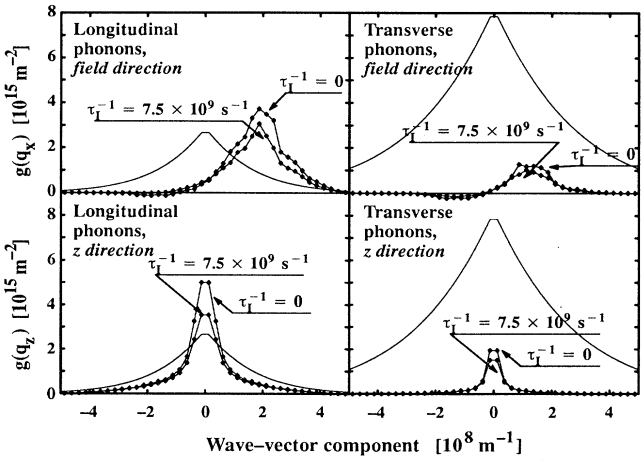

FIG. 5. The same as in Fig. 3 for $N_W = 36$, but the result obtained for $\tau_I^{-1} = 7.5 \times 10^9\ \mathrm{s}^{-1}$ is also shown. These results were obtained in the same MC run like the corresponding drift velocities in Fig. 4.

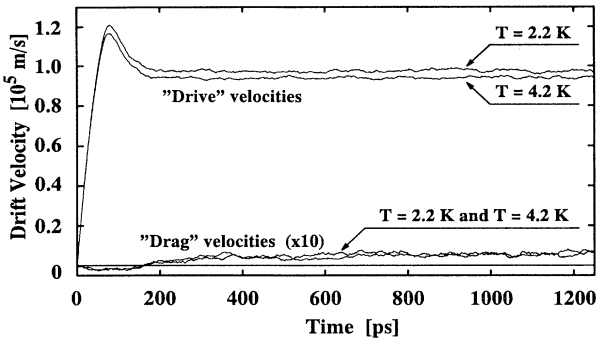

FIG. 6. Drift velocity vs time in the MQW at 4.2 K and 2.2 K for $N_W = 36$ and $\tau_I^{-1} = 7.5 \times 10^9$ s^{-1}. 60 000 particles per channel were simulated here. Other parameters and notations are given in the text of Fig. 2.

the momentum transfer rate τ_d^{-1} remains nearly the same ($\sim 1.5\times10^6$ s^{-1}). These results differ from those obtained for Ohmic conditions,[12] where the phonon drag steeply decreases with T due to the onset of Bloch-Grüneisen regime, i.e., due to thermal ceasing of the phonons with $q \simeq 2k_F$. A fundamentally different behavior of the hot phonon distributions can be seen in Fig. 7. g is almost the same for both temperatures, because it is determined mainly by spontaneous phonon emission, which is not affected by lattice temperature. Thus, thermal ceasing of nonequilibrium phonons does not appear, although the Bose distribution significantly decreases with T. Since the difference between the electron mobilities at 2.2 K and 4.2 K is small, the "drag" velocities in Fig. 6 are close.

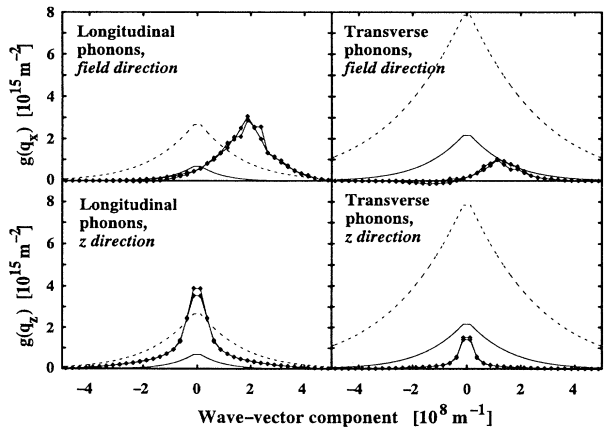

FIG. 7. Acoustic-phonon distribution vs phonon-wave vector in the field direction (q_x) and z direction (q_z) at 2.2 K and 4.2 K. Equilibrium Bose distribution n_0 is shown in a full line (2.2 K) and in a dashed line (4.2 K). Nonequilibrium part g of the distribution is shown with centered symbols. Curves for 2.2 K and 4.2 K are not distinguished, because g is almost the same for both temperatures.

IV. NONEQUILIBRIUM PHONONS AND TAP DRAG IN THIN SAMPLES

In thin samples with $L_s \ll l_{\rm ph}$, one has to consider multiple-phonon reflections from sample surfaces as well as the finite lifetime $\tau = l_{\rm ph}/v_s$. Transport equation for phonons in thin samples reads[34]

$$v_z \frac{d}{dz} g(\mathbf{q}, z) + \frac{g(\mathbf{q}, z)}{\tau} = \left\langle \frac{\partial}{\partial t} g(\mathbf{q}, z) \right\rangle_{\text{ph-el}}, \tag{22}$$

where $\langle \partial g/\partial t \rangle_{\text{ph-el}}$ is the phonon-electron collisional integral. Equation (22) holds for both longitudinal ($v_s = v_l$) and transversal ($v_s = v_t$) phonons, where v_l and v_t are the corresponding phonon velocities (for simplicity, we assume the same $l_{\rm ph}$ for both phonon branches). It is problematic to apply (22) to the structure in Fig. 1, due to the z dependence of g within the quantum well. One cannot introduce z dependent g into the 2D electron-phonon scattering rate (7,8), because 2D electrons have no exact values for z and k_z, i.e., they cannot have z dependent scattering rate. The same problem appears, when $g(\mathbf{q}, z)$ enters into $\langle \partial g/\partial t \rangle_{\text{ph-el}}$. In our simulations, typical phonon-transit times, $L_W/\mid v_z \mid \approx 10^{-11}$ s, are two orders of magnitude shorter than the typical time necessary for the phonon to be absorbed in the quantum well. That means that g varies with z negligibly on the length scale L_W. Since $l_{\rm ph} \gg L_B$, g changes negligibly also on the length scale $L_W + L_B$. In these conditions, the semiclassical model (22) should be justified and the mentioned z dependence can be kept or neglected at will. We rewrite (22) into the integral form

$$g(\mathbf{q}, z) = \exp\left(\frac{z}{v_z\tau}\right) \left\{ c(\mathbf{q}) + \frac{1}{v_z} \int_0^z dz' \exp\left(\frac{z'}{v_z\tau}\right) \times \left\langle \frac{\partial}{\partial t} g(\mathbf{q}, z') \right\rangle_{\text{ph-el}} \right\}, \tag{23}$$

where $c(\mathbf{q}) = g(\mathbf{q}, z = 0)$. Then we replace $\langle \partial g/\partial t \rangle_{\text{ph-el}}$ inside the lth quantum well by the z-independent function,

$$\frac{1}{L_W} G_l(\mathbf{q}) \equiv \left\langle \frac{\partial}{\partial t} g_l(\mathbf{q}) \right\rangle_{\text{ph-el}}, \tag{24}$$

where

$$g_l(\mathbf{q}) = \frac{1}{L_W} \int_{z_l - L_W/2}^{z_l + L_W/2} dz\; g(\mathbf{q}, z) \tag{25}$$

and $G_l(\mathbf{q})$ is given by (19). Outside each quantum well, we set

$$\left\langle \frac{\partial}{\partial t} g(\mathbf{q}, z) \right\rangle_{\text{ph-el}} = 0, \tag{26}$$

assuming that there are no free carriers in the $Al_xGa_{1-x}As$ barriers. Assuming elastic phonon reflections from the interfaces $z = 0$ and $z = L_s$, we adopt boundary conditions,[34]

$$g^{>}(\mathbf{q}, z = 0) = P_1\; g^{<}(q_x, q_y, -q_z, z = 0) + (1 - P_1)\; g_0^{>}(q, z = 0), \tag{27}$$

$$g^{<}(\mathbf{q}, z = L_s) = P_2\, g^{>}(q_x, q_y, -q_z, z = L_s) + (1 - P_2)\, g_0^{<}(q, z = L_s)\ . \quad (28)$$

Here, P_1 and P_2 are the probabilities of specular phonon reflection from the interfaces $z = 0$ and $z = L_s$, respectively, notations $^{>}$ and $^{<}$ hold for $q_z > 0$ and for $q_z < 0$, respectively, and $g_0^{>}(q, z = 0)$ and $g_0^{<}(q, z = L_s)$ are spherically symmetric parts of $g^{>}(\mathbf{q}, z = 0)$ and $g^{<}(\mathbf{q}, z = L_s)$, which appear due to diffusive phonon reflections at the interfaces. In present calculations, we use (27) and (28) with $g_0^{>} = g_0^{<} = 0$ for simplicity. Diffusively reflected phonons could, in part, reduce electron mobility when absorbed in the quantum well, but they would not contribute to the TAP drag.

Using (24)–(28) and neglecting $G_1(\mathbf{q})$ (due to the same reason as in Sec. III), we get from (23) for $z < z_2 - L_W/2$ distributions g, which can be used in the drag channel. They read

$$g^{>}(\mathbf{q}, z) = c^{>}(\mathbf{q}) \exp\left(\frac{-z}{|\, v_z\, |\, \tau}\right)\ ,$$
$$g^{<}(\mathbf{q}, z) = c^{<}(\mathbf{q}) \exp\left(\frac{z}{|\, v_z\, |\, \tau}\right)\ , \quad (29)$$

where

$$c^{<}(\mathbf{q}) = \frac{\tau}{L_W}\left[\exp\left(\frac{L_W}{2\,|\, v_z\, |\, \tau}\right) - \exp\left(\frac{-L_W}{2\,|\, v_z\, |\, \tau}\right)\right]\left[1 - P_1 P_2 \exp\left(\frac{-2L_s}{|\, v_z\, |\, \tau}\right)\right]^{-1} \times \sum_{l=2}^{N_W}\left[G_l^{<}(\mathbf{q}) \exp\left(\frac{-z_l}{|\, v_z\, |\, \tau}\right) + P_2 \exp\left(\frac{-2L_s}{|\, v_z\, |\, \tau}\right) G_l^{>}(q_x, q_y, -q_z) \exp\left(\frac{z_l}{|\, v_z\, |\, \tau}\right)\right], \quad (30)$$

and

$$c^{>}(\mathbf{q}) = P_1\, c^{<}(q_x, q_y, -q_z)\ . \quad (31)$$

Exponential dependences on z and z_l can be neglected (replaced by 1) for $|\, v_z\, | > 10 z_l/\tau$. Also the exponential dependence on L_W disappears for $|\, v_z\, | > 10 L_W/(2\tau)$. Then (29) reduces to simple expressions,

$$g^{>}(\mathbf{q}) = \frac{P_1}{|\, v_z\, |}\left[1 - P_1 P_2 \exp\left(\frac{-2L_s}{|\, v_z\, |\, \tau}\right)\right]^{-1} \times \sum_{l=2}^{N_W}\left[G_l^{<}(q_x, q_y, -q_z) + P_2 \exp\left(\frac{-2L_s}{|\, v_z\, |\, \tau}\right) G_l^{>}(\mathbf{q})\right]\ , \quad (32a)$$

$$g^{<}(\mathbf{q}) = \frac{1}{|\, v_z\, |}\left[1 - P_1 P_2 \exp\left(\frac{-2L_s}{|\, v_z\, |\, \tau}\right)\right]^{-1} \times \sum_{l=2}^{N_W}\left[G_l^{<}(\mathbf{q}) + P_2 \exp\left(\frac{-2L_s}{|\, v_z\, |\, \tau}\right) G_l^{>}(q_x, q_y, -q_z)\right]\ , \quad (32b)$$

which do not depend on z and, therefore, they provide for the drag channel a reasonable semiclassical phonon model of the 2D electron–3D phonon scattering. For $|\, v_z\, | < 10 z/\tau$ the z dependence in (29) begins to be important and semiclassical model becomes wrong. Fortunately, this is the case only for a small part of excess phonons, because $10 z/\tau \approx v_s/400$ for typical $z \approx 1$ μm and $\tau \approx 10^{-6}$ s. We use (29) with $z = z_1$ in the drag channel for all v_z.

The phonon distribution for the drive channels can be derived in a similar way as (29). We present only the result for $N_W = 2$, since our simulation will be restricted to the case of DQW. The distribution in the drive channel, averaged using (25) with $z = z_2$, reads

$$g_{l=2}(\mathbf{q}) = c(\mathbf{q})\frac{|\, v_z\, |\, \tau}{L_W}\left[\exp\left(\frac{L_W}{2\,|\, v_z\, |\, \tau}\right) - \exp\left(\frac{-L_W}{2\,|\, v_z\, |\, \tau}\right)\right] \exp\left(\frac{\mp z_2}{|\, v_z\, |\, \tau}\right) + \tau\frac{G(\mathbf{q})}{L_W}\left\{1 \mp \frac{v_z \tau}{L_W}\left[1 - \exp\left(\frac{\mp L_W}{v_z \tau}\right)\right]\right\}\ , \quad (33)$$

where the upper sign holds for $q_z > 0$ (for $g^{>}$, $c^{>}$, and $G^{>}$) and the lower sign holds for $q_z < 0$ (for $g^{<}$, $c^{<}$, and $G^{<}$). For $|\, v_z\, | > 10 z_2/\tau$, the first term on the right-hand side of (33) becomes the same as the right-hand side of [(32a) and (32b)] with $N_W = 2$. The second term, which can be simplified to $G(\mathbf{q})/(2\,|\, v_z\, |)$, is negligible compared to the first term, when $P_1 P_2 \approx 1$ and $2L_s < |\, v_z\, | \tau$. The phonon distributions in the drag and drive channels thus differ only in case of small $|\, v_z\, |$. We use (33) in the drag channel for all $|\, v_z\, |$.

The mean free path $l_{\rm ph}$ depends on N_W, due to the phonon scattering by layer interfaces. Since we consider $N_W = 2$, our $l_{\rm ph}$ should be greater than the value of 1 mm, observed for $N_W = 100$.[30] On the other hand, it should be less than the bulk value [> 5 mm (Ref. 35)]. We choose $l_{\rm ph} = 4$ mm and assume $P_1 = P_2 = P$.

In Fig. 8, we compare the TAP drag for samples with $L_s = 50$ μm and 20 μm, and $P = 1$ and 0.9. The electric field in the drive channel z_2 is 1000 V/m, the electric field in the drag channel is zero. Electron scattering with the imperfections of the host crystal is neglected ($\tau_I = 0$), in order to reduce computational time. In Fig. 9, we compare corresponding longitudinal acoustic-phonon distributions, which are responsible for the TAP drag. When $P = 1$, the drag velocity is larger for $L_s = 20$ μm than for $L_s = 50$ μm. This is due to the more effective confinement of nonequilibrium phonons in the thinner sample,

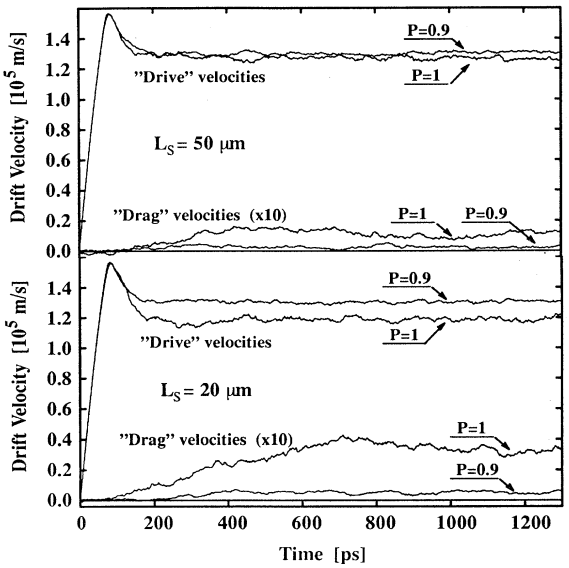

FIG. 8. Drift velocity vs time in the DQW at 4.2 K for samples with $L_s = 50$ μm and 20 μm and $P = 1$ and 0.9. Quantum well z_2 is with a parallel field $F = 1000$ V/m, quantum well z_1 is without electric field. "Drive" velocity is the velocity in the well z_2, "drag" velocity (extended by 10) is the velocity in the well z_1. The results were obtained for $\tau_I^{-1} = 0$. For $P = 0.9$, we simulated 22 500 particles per channel, for $P = 1$ only 10 000 particles per channel.

which results in the larger g (Fig. 9). When $P = 0.9$, excess phonons undergo about ten specular reflections and after that they are diffusively scattered from the drifted phonon distribution g into the spherically symmetric phonon distribution g_0 [see boundary conditions (27) and (28)], which does not contribute to the TAP drag. Therefore the "drag" velocities are much lower for

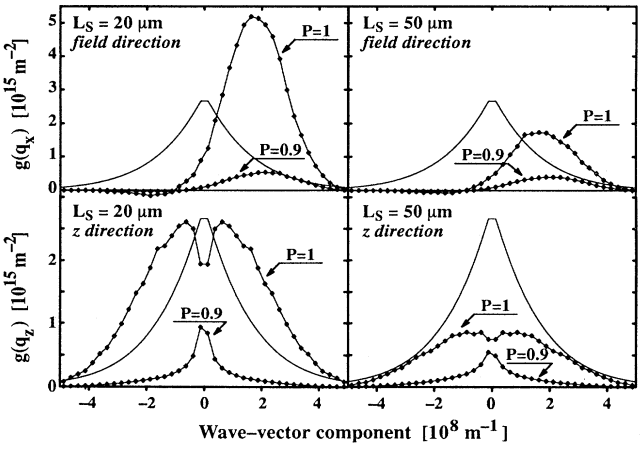

FIG. 9. Longitudinal acoustic-phonon distribution vs phonon-wave vector in the field direction (q_x) and z direction (q_z), obtained in the same MC run like corresponding drift velocities in Fig. 8. Equilibrium Bose distribution n_0 is shown in a full line, nonequilibrium part g of the distribution is shown by centered symbols.

$P = 0.9$ than for $P = 1$. The frictional effect on the "drive" velocity, discussed in Sec. III, is clearly seen in Fig. 8 for $L_s = 20$ μm. According to Figs. 8 and 9, the TAP drag in thin samples is expected to be very sensitive to the quality of sample surfaces.

To extend this calculation to thin samples with MQW's, it is convenient to replace $G_l(\mathbf{q})$ in (29) by l independent $G(\mathbf{q})$ in order to reduce the number of simulated drive channels from $N_W - 1$ to 1. Due to the negligible z dependence of g, (29) can be used also in the drive channel. Finally, when $L_s \to \infty$ and $P = 1$, one returns back to the situation simulated in Sec. III. Using the distribution (29) instead of the distribution (20), we have found about 20% larger "drag" velocities than those in Fig. 2, where excess phonons with $| v_z | < v_s/20$ were ignored. Distribution (20) is recovered from [(32a) and (32b)] for $L_s \to \infty$ and $P = 1$, when one assumes the same $G(\mathbf{q})$ and $G^< = G^>$ in each drive channel.

V. LIMITATIONS OF THE MODEL

We have assumed that only the lowest energy subband is occupied. It is easy to estimate the electron density in the first excited subband, $n_s^{\rm exc}$, assuming heated Fermi distribution at electron temperature T_e. In our simulations, we have typically $T_e \approx 50$ K in the drive channels. In the 20-nm rectangular quantum well of the 0.2-eV depth, one finds $n_s^{\rm exc} = 0.0017 n_s$, where $n_s = 1.5 \times 10^{11}$ cm^{-2}. Since $n_s^{\rm exc} \ll n_s$ and since intersubband scattering is much less frequent than intrasubband scattering,[25,27] we neglect higher subbands. For higher fields and/or for wider wells a multisubband model should be used.

We have also neglected real-space electron transfer (RSET). RSET is usually considered[36] in GaAs/$Al_xGa_{1-x}As$ quantum wells for parallel electric fields two orders of magnitude higher than our field. In measurements of the drag effect, the RSET can cause parasitic leakage currents between the drag and drive channels. In Ref. 4, the Coulomb drag in the GaAs/$Al_xGa_{1-x}As$ system was measured at lattice temperatures up to 140 K and electric field up to 10^4 V/m, and leakage currents were insignificant. Since we are dealing with much lower temperatures and fields, we believe that RSET is negligible also in our case.

We have assumed that acoustic phonons in the MQW structure are the same as in bulk GaAs, although frequency minibands may, in principle, appear in the phonon dispersion due to the "superlattice" effect. The bulk phonon approximation seems to work well in the transport analysis of the MQW structures,[30,37] with smaller superlattice period than our one. We, therefore, believe that it works well also in our case. (Our $L_W + L_B = 220$ nm is one order of magnitude larger than typical wavelength of excess phonons.) The phonons can also be incoherently scattered by superlattice interfaces. This effect is included in the phenomenological mean free path $l_{\rm ph}$, which is likely sample dependent. For thick samples with $L_s > l_{\rm ph}$ (Sec. III), the exact knowledge of $l_{\rm ph}$ is not necessary as long as $l_{\rm ph} > d_c \gg z_{N_W}$, because the phonons cross the active region of the device without

being scattered by nonelectronic scatterers. In thin samples with highly polished surfaces (Sec. IV), the results depend on $l_{\rm ph}$. We have chosen $l_{\rm ph} = 4$ mm in order to obtain quantitative insight for case $N_W = 2$, but the interpretation of the TAP drag in a specific sample would require an independent experimental determination[30,37] of $l_{\rm ph}$.

Finally, the semiclassical approach to the 2D electron–3D nonequilibrium phonon coupling is justified for phonon distributions with negligible z dependence within the quantum well. For phonons with small v_z the z dependence is important, because they are localized near the quantum well. In this case, a quantum approach should be used perhaps in a similar way as for polar-optic phonons,[38] which remain localized near the quantum well due to their small group velocities. Nevertheless, in realistic samples the "small v_z" phonons can be expected to leave the region between the contacts without crossing the drag channel, i.e., without contributing to the TAP drag. As discussed in Sec. III, a rigorous exclusion of these phonons from the phonon distribution g would remove the z dependence, but the dependence on phonon position between the contacts would appear.

Physical conditions considered in our simulations are experimentally realizable. The MQW and DQW structures with similar electron mobilities and densities have already been realized.[10,18] Thin samples with high-quality surfaces (with P close to 1) have been reported as well.[30] Due to the large spacing (200 nm) between the quantum wells in Fig. 1, it should be less complicated to prepare separate contacts to the 2D gases than in previous measurements[10] with the 20-nm spacing. Thus, we believe that the TAP drag effects predicted by our simulation could be observed.

VI. SUMMARY

We have developed low-temperature MC simulation of the TAP drag between 2D electron gases in $GaAs/Al_xGa_{1-x}As$ systems. When the MQW structure is considered, the TAP drag current increases linearly with the number of the drive channels and the exchange of hot acoustic phonons between the drive channels causes the friction of hot electrons (Fig. 2). Unlike to Ohmic conditions,[10–12] the TAP drag in hot electron conditions is mainly due to the deformation-potential coupling and its dependence on lattice temperature is negligible in the Bloch-Grüneisen regime (Figs. 6 and 7). This might provide a new probe for the deformation-potential D, which is rather problematic to determine from mobility measurements.[23] Momentum transfer rate $\tau_d^{-1} \approx 1.5 \times 10^6$ s^{-1} is much larger than the one estimated in Ohmic conditions [$\sim 5 \times 10^5$ s^{-1} at 4.2 K and $\sim 1.3 \times 10^5$ s^{-1} at 2.2 K (Ref. 12)]. We have also developed MC simulation of nonequilibrium phonon effects in thin samples, where multiple-phonon reflections from sample surfaces tend to enhance the TAP drag. This effect has been demonstrated for the DQW structure (Figs. 8 and 9).

ACKNOWLEDGMENTS

M.M. was in part supported by the Comission of the European Communities, No. CIPA3510PL922838. Useful comments and technical help from Antónia Mošková and Pavol Quittner are greatly appreciated.

APPENDIX A

We intend to replace functions $|\, S_0(q_z)\,|^2$, $n(\mathbf{q})$, $C^2(\mathbf{q})$, and $\varepsilon(Q)$ in (10) by more simple functions, which ensure that the distribution $B^{\pm}(Q,\phi,k)$ obtained in this way is greater than distribution $P^{\pm}(Q,\phi,k)$. We search for proper upper limits of these functions [for the lower limit in case of $\varepsilon(Q)$]. Let $n(\mathbf{q}) = [\exp(\frac{\hbar v_s q}{k_B T}) - 1]^{-1} + g(\mathbf{q})$, where $g(\mathbf{q})$ is a nonequilibrium contribution to the Bose distribution. Choosing a large enough $T_f > T$, we may assume for any $g(\mathbf{q})$ without poles, that $n(\mathbf{q}) < [\exp(\frac{\hbar v_s q}{k_B T_f}) - 1]^{-1}$. Then one finds

$$n(\mathbf{q}) < \frac{k_B T_f}{\hbar v_s q} , \tag{A1}$$

$$n(\mathbf{q}) < 2\Big(\frac{k_B T_f}{\hbar v_s q}\Big)^2 < 2\Big(\frac{k_B T_f}{\hbar v_s Q}\Big)^2 , \tag{A2}$$

$$n(\mathbf{q}) < 6\Big(\frac{k_B T_f}{\hbar v_s q}\Big)^3 . \tag{A3}$$

From (2), one gets

$$|\, S_0(q_z)\,|^2 \le 1 . \tag{A4}$$

Function (3) has no upper limit. Functions (4) and (5) obey the inequality

$$C^2(\mathbf{q}) < C_M^2 , \tag{A5}$$

where $C_M^2 = 36(eh_{14}/\varepsilon_s)^2$ for (4) and $C_M^2 = 12(eh_{14}/\varepsilon_s)^2$ for (5). From (6), one finds that

$$\varepsilon(Q) > 1 . \tag{A6}$$

The right-hand side of (A6) is a proper lower limit in case of deformation-potential interaction. In case of piezoelectric interaction, we adopt this limit for $Q > Q^{\pm}_{\rm max}$. For $Q < Q^{\pm}_{\rm max}$, we assume

$$\varepsilon(Q) > 1 + \frac{\beta_0}{Q} \tag{A7}$$

(β_0 is a proper constant) in order to avoid divergency of piezoelectric scattering rates. It is useful to introduce notations

$$b = \frac{\hbar Q}{2mv_s} , \quad a = \frac{\hbar k}{mv_s} , \tag{A8}$$

$$b^{\pm}_{\rm min} = \frac{\hbar Q^{\pm}_{\rm min}}{2mv_s} , \quad b^{\pm}_{\rm max} = \frac{\hbar Q^{\pm}_{\rm max}}{2mv_s} , \tag{A9a}$$

which give for $a \ge 1$ equations

$$b^{\pm}_{\min} = 0 \quad , \quad b^{\pm}_{\max} = a \mp 1 \, , \tag{A9b}$$

and for $a < 1$ equations

$$b^{-}_{\min} = 1 - a \quad , \quad b^{-}_{\max} = a + 1 \, . \tag{A9c}$$

Notations (A8) allow us to express $\phi^{\pm}(Q)$ as

$$\phi^{\pm}(b) = \arccos\left(\frac{1 \pm b}{a}\right) \, . \tag{A10}$$

Finally, we introduce functions

$$f^{\pm}(\phi) = (a\cos\phi \mp b)^2 - 1 \, , \tag{A11}$$

where the $f^{+}(\phi)$ is defined for $b^{+}_{\min} < b < b^{+}_{\max}$ and $f^{-}(\phi)$ is defined for $b^{-}_{\min} < b < \infty$. As shown in Appendix B, for $b^{\pm}_{\min} < b < b^{\pm}_{\max}$ and $\phi \in \langle -\phi^{\pm}, \phi^{\pm} \rangle$, we have

$$f^{\pm}(\phi) \geq \min\left(\frac{f^{\pm}(0)}{\phi^{\pm}}, 2a\sin\phi^{\pm}\right)(\phi^{\pm} - \mid \phi \mid) \, . \tag{A12}$$

For $b > b^{-}_{\max}$ and $\phi \in \langle -\pi, \pi \rangle$ one finds

$$f^{-}(\phi) \geq (b-a)^2 - 1 \, . \tag{A13}$$

$B^{\pm}(Q,\phi,k)$ for piezoelectric interaction. We replace functions $n(\mathbf{q})$, $\mid S_0(q_z) \mid^2$ and $C^2(\mathbf{q})$ in the right-hand side of (10) by the right-hand side of (A2), (A4), and (A5), respectively. Using (A8) and (A11), we get

$$P^{\pm}(Q,\phi,k) < \left(\frac{k_B T_f}{m v_s^2}\right)^2 C_M^2 \frac{1}{\sqrt{f^{\pm}(\phi)}} \frac{1}{b^2 \varepsilon^2(b)} \times \left[1 + \left(\frac{m v_s^2}{k_B T_f}\right)^2 b^2 (1 \pm 1)\right] \, . \tag{A14}$$

For $b > b^{-}_{\max}$ ($Q > Q^{-}_{\max}$), we replace $\varepsilon(Q)$ and $f^{-}(\phi)$ in (A14) by the right-hand side of (A6) and (A13), respectively. We get

$$P^{-}(Q,\phi,k) < B^{-}(Q,\phi,k) \equiv B^{-}_{\text{piez}}(b,\phi,a) \, , \tag{A15}$$

$$B^{-}_{\text{piez}}(b,\phi,a) = \left(\frac{k_B T_f}{m v_s^2}\right)^2 C_M^2 \frac{1}{b^2\sqrt{(b-a)^2 - 1}} \, . \tag{A16}$$

For $b < b^{\pm}_{\max}$ ($Q < Q^{\pm}_{\max}$), we replace $\varepsilon(Q)$ and $f^{\pm}(\phi)$ in (A14) by the right-hand side of (A7) and (A12), respectively. We get

$$P^{\pm}(Q,\phi,k) < B^{\pm}(Q,\phi,k) \equiv B^{\pm}_{\text{piez}}(b,\phi,a), \tag{A17}$$

$$B^{\pm}_{\text{piez}}(b,\phi,a) = \left(\frac{k_B T_f}{m v_s^2}\right)^2 C_M^2 \frac{1}{(b+\beta)^2} \times \left\{1 + \left[\frac{m v_s^2}{k_B T_f}\right]^2 b^2 (1 \pm 1)\right\} \times \max\left[\sqrt{\frac{\phi^{\pm}}{f^{\pm}(0)}} \, , \, \frac{1}{\sqrt{2a\sin\phi^{\pm}}}\right] \times \frac{1}{\sqrt{\phi^{\pm} - \mid \phi \mid}} \, , \tag{A18}$$

where $\beta \equiv \hbar\beta_0 / 2 m v_s$.

$B^{\pm}(Q,\phi,k)$ for deformation-potential interaction. We replace functions $n(\mathbf{q})$, $\mid S_0(q_z) \mid^2$ and $\varepsilon(Q)$ in the right-hand side of (10) by the right-hand side of (A1), (A4), and (A6), respectively. Using (A8) and (A11), we get

$$P^{\pm}(Q,\phi,k) < \frac{4 m k_B T_f D^2}{\hbar^2} b \sqrt{\frac{f^{\pm}(\phi) + 1}{f^{\pm}(\phi)}} \left\{1 + \left[\frac{m v_s^2}{k_B T_f}\right] \times b\sqrt{f^{\pm}(\phi) + 1}(1 \pm 1)\right\} . \tag{A19}$$

Except for the denominator, we replace $f^{\pm}(\phi)$ in (A19) by $(a+b)^2 - 1$. In the denominator, we replace $f^{\pm}(\phi)$ by the right-hand side of (A12)–(A13). For $b < b^{\pm}_{\max}$ ($Q < Q^{\pm}_{\max}$), we get

$$P^{\pm}(Q,\phi,k) < B^{\pm}(Q,\phi,k) \equiv B^{\pm}_{\text{def}}(b,\phi,a) \, , \tag{A20}$$

$$B^{\pm}_{\text{def}}(b,\phi,a) = \frac{4 m k_B T_f D^2}{\hbar^2} b(a+b) \times \left\{1 + \left[\frac{m v_s^2}{k_B T_f}\right] b(a+b)(1 \pm 1)\right\} \times \max\left[\sqrt{\frac{\phi^{\pm}}{f^{\pm}(0)}} \, , \, \frac{1}{\sqrt{2a\sin\phi^{\pm}}}\right] \times \frac{1}{\sqrt{\phi^{\pm} - \mid \phi \mid}} \, , \tag{A21}$$

while for $b > b^{-}_{\max}$ ($Q > Q^{-}_{\max}$), we get

$$P^{-}(Q,\phi,k) < B^{-}(Q,\phi,k) \equiv B^{-}_{\text{def}}(b,\phi,a) \, , \tag{A22}$$

$$B^{-}_{\text{def}}(b,\phi,a) = \frac{4 m k_B T_f D^2}{\hbar^2} \frac{b(a+b)}{\sqrt{(b-a)^2 - 1}} \, . \tag{A23}$$

Function (A23) gives infinite integral $\int_{b^{-}_{\max}}^{\infty} db \int_{-\pi}^{\pi} d\phi \, B^{-}_{\text{def}}$. To avoid this, we adopt (A23) only for $b^{-}_{\max} < b < b_0$, where b_0 is chosen as $b_0 = 2b^{-}_{\max} - 1$. For $b > b_0$, we need $B^{-}_{\text{def}}(b,\phi,a)$, which gives finite integral $\int_{b_0}^{\infty} db \int_{-\pi}^{\pi} d\phi \, B^{-}_{\text{def}}$. We again substitute functions $\mid S_0(q_z) \mid^2$ and $\varepsilon(Q)$ in the right-hand side of (10) as in the derivation of (A19), but $n(\mathbf{q})$ is now replaced by the right-hand side of (A3). Using (A8) and (A11), we get

$$P^{-}(Q,\phi,k) < \frac{6\hbar D^2}{m v_s}\left(\frac{k_B T_f}{\hbar v_s}\right)^3 \frac{1}{b f^{-}(\phi)} \, . \tag{A24}$$

Replacing $f^{-}(\phi)$ in (A24) by the right-hand side of (A13) we obtain (A22) with

$$B^{-}_{\text{def}}(b,\phi,a) = \frac{6\hbar D^2}{m v_s}\left(\frac{k_B T_f}{\hbar v_s}\right)^3 \frac{1}{b[(b-a)^2 - 1]} \, . \tag{A25}$$

Generation of $\phi(r_2)$, $Q(r_1)$ and $\lambda^{\pm}$. We replace $P^{\pm}(Q,\phi,k)$ in (12)–(17) by $B^{\pm}(b,\phi,a)$. From (13), we get

$$\phi = \phi^{\pm}(b)\left[1-4r_2^2\right] \quad , \quad 0 \le r_2 \le \frac{1}{2} \, , \tag{A26a}$$

$$\phi = -\phi^{\pm}(b)\left[1-4(1-r_2)^2\right] \quad , \quad \frac{1}{2} \le r_2 \le 1 \, , \tag{A26b}$$

which are valid for $b^{\pm}_{\min} < b < b^{\pm}_{\max}$. From (17) (for absorption in case $b > b^{-}_{\max}$), we get

$$\phi = (2r_2 - 1)\pi \quad , \quad 0 \le r_2 \le 1 \, . \tag{A27}$$

From (12), we obtain

$$r_1 = \frac{\int_{b^{+}_{\min}}^{b} db\, B_1^{+}(b,a)}{\int_{b^{+}_{\min}}^{b^{\pm}_{\max}} db\, B_1^{+}(b,a)} \, , \tag{A28}$$

and from (14) and (15), we have

$$r_1 = \frac{\int_{b^{-}_{\min}}^{b} db\, B_1^{-}(b,a)}{\int_{b^{-}_{\min}}^{b^{-}_{\max}} db\, B_1^{-}(b,a) + \int_{b^{-}_{\max}}^{\infty} db\, B_2^{-}(b,a)} \, , \quad b \le b^{-}_{\max} \, , \tag{A29}$$

$$r_1 = \frac{\int_{b^{-}_{\min}}^{b^{-}_{\max}} db\, B_1^{-}(b,a) + \int_{b^{-}_{\max}}^{b} db\, B_2^{-}(b,a)}{\int_{b^{-}_{\min}}^{b^{-}_{\max}} db\, B_1^{-}(b,a) + \int_{b^{-}_{\max}}^{\infty} db\, B_2^{-}(b,a)} \, , \quad b > b^{-}_{\max} \, , \tag{A30}$$

where

$$B_1^{\pm}(b,a) = \int_{-\phi_0^{\pm}(b)}^{\phi_0^{\pm}(b)} d\phi B^{\pm}(b,\phi,a), \quad b^{\pm}_{\min} < b < b^{\pm}_{\max} \, , \tag{A31}$$

$$B_2^{-}(b,a) = \int_{-\pi}^{\pi} d\phi B^{-}(b,\phi,a) \quad , \quad b > b^{-}_{\max} \, , \tag{A32}$$

with notations "piez" and "def" omitted. Integrals (A31) and (A32) can be calculated analytically. Equations (A28)–(A30) yield $b = b(r_1)$ $[Q = Q(r_1)]$ after some numerical work, including numerical tabulation of the involved integrals. Finally, replacing $P^{\pm}$ by $B^{\pm}$ in (7,8), a new $\lambda^{\pm}$ can be evaluated by numerical integration.

APPENDIX B

To prove inequality (A12) it is sufficient to consider $\phi \ge 0$, because $f^{\pm}(\phi) = f^{\pm}(-\phi)$. For $\phi \in \langle 0, \phi^{\pm}\rangle$ function $f^{\pm}(\phi)$ is positive, with maximum

$$f^{\pm}(0) = (a \mp b)^2 - 1 \, , \tag{B1}$$

and with minimum

$$f^{\pm}(\phi^{\pm}) = 0 \, . \tag{B2}$$

Since $d^2 f^{\pm}(0)/d^2\phi < 0$, $f^{\pm}(\phi)$ is concave at least for ϕ close to zero. Solving equation $d^2 f^{\pm}(\phi)/d^2\phi = 0$, one finds inflex points $\phi^{\pm}_{i_1}$ and $\phi^{\pm}_{i_2}$, given as

$$\cos\phi^{\pm}_{i_1} = \frac{\pm b + \sqrt{b^2+8a^2}}{4a} \, , \quad \cos\phi^{\pm}_{i_2} = \frac{\pm b - \sqrt{b^2+8a^2}}{4a} \, . \tag{B3}$$

It is easy to see that $\phi^{\pm}_{i_2} > \phi^{\pm}$ (check that $\cos\phi^{\pm}_{i_2} < \cos\phi^{\pm}$), i.e., that only $\phi^{\pm}_{i_1}$ can fall into the interval $\langle 0, \phi^{\pm}\rangle$.

If $\phi^{\pm}_{i_1} > \phi^{\pm}$, $f^{\pm}(\phi)$ is concave for $\phi \in \langle 0, \phi^{\pm}\rangle$ and due to (B1)–(B2), we have

$$f^{\pm}(\phi) \ge \frac{f^{\pm}(0)}{\phi^{\pm}}(\phi^{\pm} - \phi) \, . \tag{B4}$$

If $\phi^{\pm}_{i_1} \in \langle 0, \phi^{\pm}\rangle$, then $f^{\pm}(\phi)$ is concave only for $\phi \in \langle 0, \phi^{\pm}_{i_1}\rangle$ and (B4) holds only if

$$\frac{f^{\pm}(0)}{\phi^{\pm}} \le -\frac{df^{\pm}(\phi^{\pm})}{d\phi} \, , \tag{B5}$$

where $df^{\pm}(\phi^{\pm})/d\phi = -2a\,\sin(\phi^{\pm})$. If (B5) does not hold, then

$$f^{\pm}(\phi) \ge -\frac{df^{\pm}(\phi^{\pm})}{d\phi}(\phi^{\pm} - \phi) \, . \tag{B6}$$

Finally, from (B4)–(B6) and from $f^{\pm}(\phi) = f^{\pm}(-\phi)$, we obtain (A12).

*Permanent address: Institute of Electrical Engineering of SAS, Dúbravská cesta 9, 842 39 Bratislava, Slovakia.

[1] K. Hubner and W. Shockley, Phys. Rev. Lett. **4**, 504 (1960).
[2] M.B. Pogrebinskii, Fiz. Tekh. Poluprovodn. **11**, 637 (1977) [Sov. Phys. Semicond. **11**, 372 (1977)].
[3] P.J. Price, Physica **117B**, 750 (1983).
[4] P.M. Solomon, P.J. Price, D.J. Frank, and D.C. La Tulipe, Phys. Rev. Lett. **63**, 2508 (1989).
[5] B. Laikhtman and P.M. Solomon, Phys. Rev. B **41**, 9921 (1990).
[6] D.L. Maslov, Phys. Rev. B **45**, 1911 (1992).
[7] I.I. Boiko, P. Vasilopoulos, and Yu.M. Sirenko, Phys. Rev. B **45**, 13 538 (1992).
[8] H.C. Tso and P. Vasilopoulos, Phys. Rev. B **45**, 1333 (1992).
[9] Yu.M. Sirenko and P. Vasilopoulos, Phys. Rev. B **46**, 1611 (1992).
[10] T.J. Gramila, J.P. Eisenstein, A.H. MacDonald, L.N. Pfeiffer, and K.L. West, Phys. Rev. Lett. **66**, 1216 (1991).
[11] T.J. Gramila, J.P. Eisenstein, A.H. MacDonald, L.N. Pfeiffer, and K.L. West, Surf. Sci. **263**, 446 (1992).
[12] T.J. Gramila, J.P. Eisenstein, A.H. MacDonald, L.N. Pfeifer, and K.L. West, Phys. Rev. B **47**, 12 957 (1993).
[13] H.C. Tso, P. Vasilopoulos, and F.M. Peeters, Phys. Rev.

Lett. **68**, 2516 (1992).
[14]V. Sivan, P.M. Solomon, and H. Strikman, Phys. Rev. Lett. **68**, 1196 (1992).
[15]H.C. Tso, P. Vasilopoulos, and F.M. Peeters, Phys. Rev. Lett. **70**, 2146 (1993).
[16]H. Karl, W. Dietsche, A. Fisher, and K. Ploog, Phys. Rev. Lett. **61**, 2360 (1988)
[17]P.J. Price, Physica **134B**, 164 (1985).
[18]L.N. Pfeiffer, K.W. West, J.P. Eisenstein, K.W. Baldwin, and P. Gammel, Appl. Phys. Lett. **61**, 1211 (1992).
[19]M. Moško and A. Mošková, Phys. Rev. B **44**, 10 794 (1991).
[20]A. Mošková and M. Moško, Phys. Rev. B **49**, 7443 (1994).
[21]M. Moško, V. Cambel, and A. Mošková, Phys. Rev. B **46**, 5012 (1992).
[22]V. Cambel and M. Moško, Semicond. Sci. Technol. **8**, 364 (1993).
[23]H.L. Stormer, L.N. Pfeiffer, K.W. Baldwin, and K.W. West, Phys. Rev. B **41**, 1278 (1990).
[24]P. Lugli and D.K. Ferry, IEEE Trans. Electron. Devices **ED-32**, 2431 (1985).
[25]M. Artaki and K. Hess, Phys. Rev. B **37**, 2933 (1988).
[26]B.K. Ridley, *Quantum Processes in Semiconductors* (Clarendon, Oxford, 1982).
[27]K. Yokoyama and K. Hess, Phys. Rev. B **33**, 5595 (1986).
[28]J.S. Blakemore, J. Appl. Phys. **53**, R123 (1982).
[29]M. Moško, J.L. Pelouard, and F. Pardo, Semicond. Sci. Technol. **9**, 806 (1994).
[30]V. Bayot, M.B. Santos, and M. Shayegan, Phys. Rev. B **46**, 7240 (1992).
[31]M. Rieger, P. Kocevar, P. Lugli, P. Bordone, L. Regiani, and S.M. Goodnick, Phys. Rev. B **39**, 7866 (1989).
[32]P. Bordone, C. Jacoboni, P. Lugli, L. Reggiani, and P. Kocevar, J. Appl. Phys. **61**, 1460 (1986).
[33]S.K. Lyo, Phys. Rev. B **43**, 2412 (1991).
[34]J.M. Ziman, *Electrons and Phonons* (Clarendon Press, Oxford, 1963).
[35]M.I. Newton, V.W. Rampton, P.J.A. Carter, M. Henini, and O.H. Hughes, in *Proceedings of the 19th International Conference on the Physics of Semiconductors*, edited by W. Zawadski (Institute of Physics, Polish Academy of Sciences, Warsaw, 1988), p. 335.
[36]M. Moško and I. Novák, J. Appl. Phys. **67**, 890 (1990).
[37]J.P. Eisenstein, A.C. Gossard, and V. Narayanamurti, Phys. Rev. Lett. **59**, 1341 (1987).
[38]W.Cai, M.C. Marchetti, and M. Lax, Phys. Rev. B **34**, 8573 (1986).